

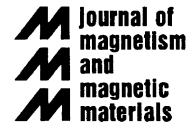


ELSEVIER

Available online at www.sciencedirect.com

SCIENCE @ DIRECT®

Journal of Magnetism and Magnetic Materials 288 (2005) 196–204



www.elsevier.com/locate/jmmm

Micromagnetic studies of nickel microbars fabricated by nanoimprint lithography and electrodeposition

Darko Grujicic, Batric Pesic*

Department of Materials Science and Engineering, University of Idaho, McClure Hall, Moscow, ID 83844-3024, USA

Received 16 June 2004; received in revised form 7 August 2004

Available online 5 October 2004

Abstract

Micromagnetic configurations and macromagnetic properties of electrodeposited nickel microbars with six different aspect ratios defined by nanoimprint lithography, and their magnetization switching properties along the long axis were investigated. It was found that the magnetization direction depends on the thickness of nickel microbars. In the remanent state, magnetization in microbars with smaller aspect ratios had a predominantly vortex configuration, while microbars with higher aspect ratios were predominantly in a single-domain state. Individual remanent curves, extracted from magnetic force microscopy images for microbars with all aspect ratios, show that in the range of magnetic fields investigated, complete switching of magnetization takes place only in microbars with aspect ratios larger than 2.86. Individual remanent curves were used to construct the net remanent curve, and its agreement with the macroscopic remanent magnetization curve is discussed. The switching mechanism of nickel microbars with rounded corners proceeds through vortex formation, as determined by micromagnetic modeling.

© 2004 Elsevier B.V. All rights reserved.

PACS: 75.50.Cc; 75.75.+a; 81.15.Pq

Keywords: Electrodeposited nickel; Magnetic microbar; Magnetic vortex; Magnetization reversal; Magnetic force microscopy–MFM

1. Introduction

In recent years, there has been considerable interest in the study of switching properties of ferromagnetic elements for their application in magnetic random access memory (MRAM) [1].

Among the ferromagnetic metals and alloys used for preparation of sub-micron elements suitable for studies of magnetic switching properties, nickel is most often used as Ni–Fe alloy (permalloy) [2–4]. The exceptions are ferromagnetic elements with perpendicular magnetization, where great attention has been paid to the magnetic properties of nickel nanowires, most often prepared by electrodeposition methods [5–9]. The study of in-plane magnetization reversal in single-domain

*Corresponding author. Tel.: +208 885 6569; fax: +208 885 2855.

E-mail address: pesic@uidaho.edu (B. Pesic).

elements requires that the magnetization lies parallel to the plane of the substrate. In comparison to many studies of cobalt and permalloy, the number of micromagnetic studies relevant to nickel elements with in-plane magnetization is rather limited (Ref. [10] being one of the few). However, in these studies, the electrodeposition methods that are so suitable for studying nickel nanowires were generally replaced with vacuum deposition techniques to produce elements with in-plane magnetization.

This paper describes the results of micromagnetic (MFM) and macromagnetic (VSM) studies of nickel microbars with round corners, produced by nanoimprinting and electrodeposition. Among the parameters studied were: the effect of microbar thickness, and the effect of the microbar's length-to-width aspect ratio, as well as the effect of edge roughness on the switching field range and the associated switching mechanisms. The results of theoretical micromagnetic simulations are also included.

2. Experimental

Nickel microbars were produced by a procedure that involved nanoimprinting of a digital versatile disc (DVD) stamp into a polymethylmethacrylate (PMMA) layer spun on a (1 0 0) silicon wafer with a 50 nm sputtered copper seed layer, reactive ion etching of the excess PMMA to expose the underlying copper film, electrodeposition of nickel into patterned voids, and finally removal of the remaining PMMA. The procedure is described in detail elsewhere [11]. The composition of the solution was 0.05 M NiSO₄ and 0.5 M H₃BO₃, with no other additives present. Electrodeposition was carried out at -1100 mV vs. Ag/AgCl reference electrode ($E_{\text{H}}^0 = +0.222$ V). Samples of two different thicknesses were prepared: 55 nm- and 12 nm-thick nickel microbars, electrodeposited for 30 and 10 s, respectively. The DVD stamp used for patterning contained microbars with six length-to-width aspect ratios (AR): 1.43, 2.14, 2.86, 3.57, 4.26, and 5.00. The width of all microbars was 700 nm. Separation between the

individual microbars was at least 1000 nm in all directions.

Magnetic properties of nickel microbars were investigated on a macroscale by a vibrating sample magnetometer (VSM; ADE DMS model 886), and on a microscale by magnetic force microscopy (MFM; VEECO DI Nanoscope IIIa, MultiMode, frequency modulation, regular or low moment Co–Cr-coated MFM tips, VEECO).

3. Results and discussion

3.1. Nickel crystallography

Nickel thin films grown pseudomorphically on a copper lattice exhibit very peculiar magnetic properties [12]. Both nickel and copper have face-centered cubic (FCC) lattices, with a lattice mismatch of 2.5%. The difference in lattice parameters results in lattice strain at the interface between copper and nickel. Lattice strain affects the magnetic properties of nickel in such a way that it changes the sign of the bulk magnetocrystalline anisotropy constant from negative to positive in the thickness range between 20 and 135 Å, shifting the easy axis of magnetization from parallel-to-plane to perpendicular-to-plane [12]. The MFM images of deposited nickel elements with 55 and 12 nm thicknesses, taken at remanence after saturation at 600 and 1400 Oe, respectively, are presented in Fig. 1a and b. Each image includes nickel microbars of several aspect ratios.

According to Fig. 1a, after applying a field of 600 Oe all of the 55 nm-thick microbars retained a single-domain state at the remanence. Additional contrast changes that appear along the edges of the longer microbars are a result of the edge domain formation due to the edge roughness. The image in Fig. 1b shows that the remanent state of 12 nm-thick microbars is not a single-domain state even after magnetization at 1400 Oe, as evidenced by numerous alternating bright and dark areas. Because the thickness of the nickel microbars studied falls within the 20–135 Å range, a strong out-of-plane magnetization component [12] could explain the observed multiple contrasts in the MFM image. Additionally, because

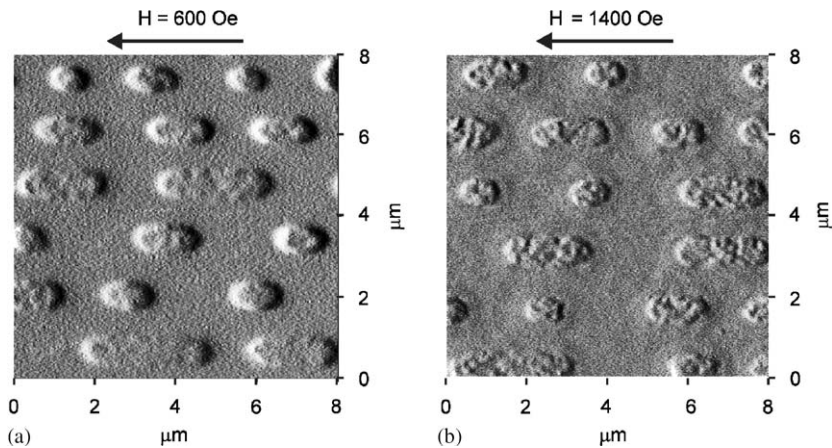


Fig. 1. MFM images of (a) 55 nm- and (b) 12 nm-thick nickel microbars after application of specified magnetic fields. The images represent phase modulations of an oscillating, low moment MFM tip (constant height mode with 100 nm lift height; vertical scale 2°).

electrodeposition of nickel is always accompanied by hydrogen reduction, the consequent hydrogen atom adsorption may further complicate the magnetocrystalline anisotropy of nickel films [13].

In order to determine the in-plane and out-of-plane magnetization components of the nickel microbars deposited in this study, a related VSM study was performed on the samples corresponding to the MFM images presented in Fig. 1a and b. The VSM results are presented in Fig. 2a and b. In-plane magnetization curves were recorded with the longer axes of microbars parallel to the applied magnetic field, as schematically indicated in the insets.

According to the magnetization curve of 55 nm-thick nickel microbars, Fig. 2a, magnetization lies parallel to the plane of the substrate. In 12 nm-thick microbars, however, there was a significant component of magnetization perpendicular to the film's surface, Fig. 2b. A strong magnetic component perpendicular to the substrate results in magnetic moments which alternate in upward and downward directions, producing the bright–dark contrast seen in the MFM image, Fig. 1b. It follows that the nickel microbars in the 20–135 Å thickness range are unsuitable for studies of single-domain in-plane magnetization reversal. Consequently, 12 nm-thick nickel microbars were eliminated from further study.

3.2. Effect of aspect ratio on switching field distribution—MFM remanent magnetization curves

In order to investigate the extent of shape anisotropy on the switching properties of nickel microbars, the sample was first subjected to a magnetic field of +600 Oe, applied parallel to the long axis of the microbars. The field was then reversed to a certain reverse field H_{rev} , and subsequently shut off. Remanent magnetization curves were then extracted from MFM images in the following manner: microbars with a linear single-domain state in the direction of the saturation field were assigned a value of +1, while the ones with a linear single-domain state in the direction parallel to the direction of the reverse field were assigned a value of –1. Microbars with a low magnetic contrast in MFM images, stemming from the domain closure within the microbars, were assigned a value of zero. The method of constructing the curves was described earlier [11].

Fig. 3a, and b indicates that AR 1.43 and 2.14 microbars did not achieve uniform single-domain magnetization in the investigated range of reverse fields. After field reversal to –600 Oe, only about 20% of AR 1.43 microbars were in a single-domain state at the remanence, Fig. 3a, compared to about 60% for microbars with AR 2.14, Fig. 3b. The higher fraction of single-domain bars with

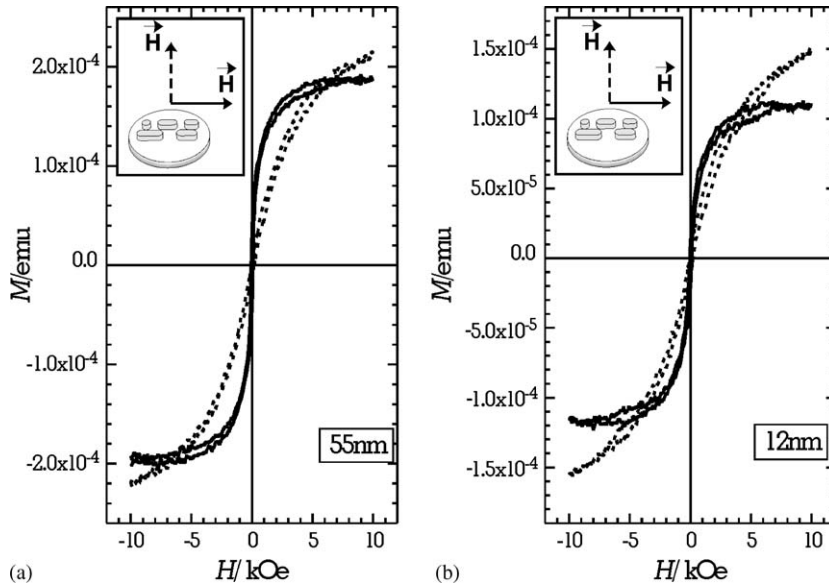


Fig. 2. (a,b) VSM magnetization curves of nickel microbars with thicknesses of 55 nm (a) and 12 nm (b). In-plane and out-of-plane magnetization curves are presented by full and dashed lines, respectively.

increased AR is a consequence of larger shape anisotropy.

Before the onset of switching, at 0 Oe, most of the AR 2.86 microbars were in a single-domain state parallel to the saturation field, Fig. 3c. When the switching was finished at reverse fields higher than -200 Oe, a fraction (3–5%) of microbars still remained in a demagnetized remanent state. Consequently, the microbars with this aspect ratio were never found entirely in a single-domain state. Microbars with aspect ratios higher than 2.86, Fig. 3d–f, all switched their single-domain orientations within the range of applied reverse fields and all retained single-domain state at the remanence.

The magnitude of the magnetic fields of microbars was calculated [14] in order to estimate the effect of dipolar coupling between the microbars in the remanent state. The strongest dipole field would result from the longest microbar with AR 5.00. By approximating an AR 5.00 microbar with a dipole of $3.5\ \mu\text{m}$ length, the calculated field emanating from the bar and acting at a distance of $1\ \mu\text{m}$ was 18 Oe. This is lower than the measured coercivity of the microbars, so the effect of dipolar coupling at the remanence was negligible.

3.3. Switching field distribution

Fig 3a–f shows that the width of the switching field distribution depends on the aspect ratio of the microbars. In order to determine the distribution of the switching fields, experimental points in Figs. 3a–f were fitted with Boltzman-type sigmoidal curves (solid lines in Figs. 3a–f). Fitted curves were then differentiated with respect to the applied field and fitted with Gaussian distributions. Two standard deviations (2σ) of the switching field distribution were then determined from the full-width at half-maximum (FWHM) of the peak on the dM/dH curve, Fig. 4, for each aspect ratio. The width of the switching field distribution for AR 2.83 microbars was 162 Oe, although, as mentioned earlier, at least 3–5% of the microbars with this AR were always found in a demagnetized state. The width of the switching field distribution for AR 3.57, 4.26 and 5.00 was 116, 47 and 50 Oe, respectively. Within these field ranges, 95% of the microbars of the corresponding aspect ratios switched the direction of their single-domain magnetization.

The peaks on the curves are located between -110 and -120 Oe, which is slightly higher than

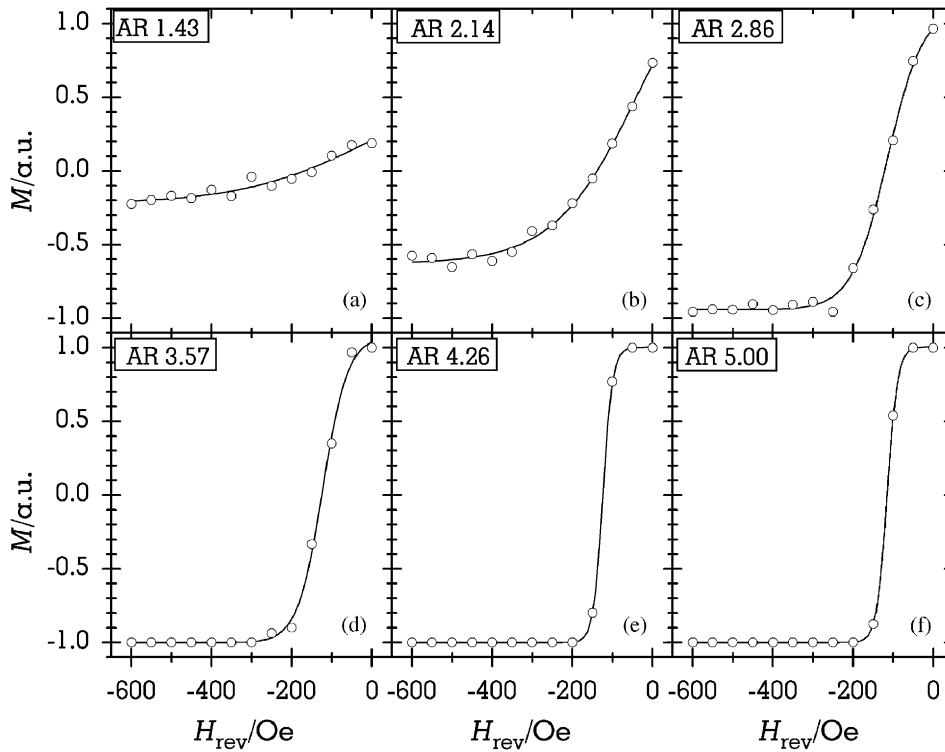


Fig. 3. (a–f) Remanent curves extracted from MFM images corresponding to nickel microbars with the following length-to-width aspect ratios: (a) 1.43, (b) 2.14, (c) 2.86, (d) 3.57, (e) 4.26, and (f) 5.00. Open circles represent experimental data; lines represent Boltzmann-type sigmoidal curve fits. Note that the microbars with two smallest aspect ratios were not saturated. For microbars with higher aspect ratios, the width of the switching field range decreased with the increase of aspect ratio.

the measured coercivity of the entire sample, about -100 Oe. The measured coercivity of continuous nickel film electrodeposited under the same conditions was 77 Oe. The higher coercivity of nickel microbars arises from their shape anisotropy.

In the range of reverse fields investigated, there is no second peak on dM/dH curves of AR 2.14 and 2.86 microbars, as was present in the study of cobalt microbars with the same aspect ratios [11]. Two peaks indicate stabilization of vortex states [11], [15], and their absence implies that the vortex states in nickel microbars with AR 2.14 and 2.86 are more unstable than in cobalt microbars of the same aspect ratio.

3.4. Switching mechanisms

In order to determine the switching mechanisms of magnetic dipoles in nickel microbars, the

coercivity of the microbars with different aspect ratios was calculated according to the Stoner–Wohlfarth coherent rotation mechanism [16]. Calculated coercivities increased with the increase of aspect ratio from 27 Oe for AR 1.43, to 250 Oe for AR 5.00 microbars. Because measured coercivities of microbars with AR 2.86 and higher were about 110 – 120 Oe and independent of aspect ratio, it follows that the reversal of magnetization direction in nickel microbars with AR equal or higher than 2.86 does not take place through coherent spin rotation. Nickel particles with a perpendicular magnetization orientation were earlier found to exhibit incoherent magnetization reversal [7]. Incoherent magnetization reversal should also be expected from a large difference in the dimensions of the microbars compared to the exchange length of nickel (7.72 nm).

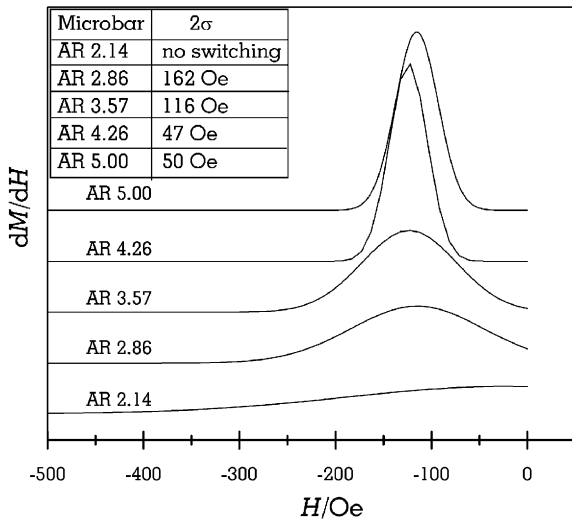


Fig. 4. Distribution of switching fields as a function of aspect ratio. The lines are derivatives of the fitting curves in Figs. 3b–f with respect to the applied field. Note the absence of a peak for nickel microbars with AR 2.14.

To further understand the magnetization switching mechanisms, a nickel microbar of AR 5.00 was selected for micromagnetic simulation utilizing the code developed by NIST [17]. The saturation magnetization used for modeling was $M_s = 4.9 \times 10^5 \text{ A m}^{-1}$, with a cell size of $10 \text{ nm} \times 10 \text{ nm} \times 55 \text{ nm}$ (film thickness). The magnetocrystalline anisotropy coefficient, K_1 , was set to zero, implying the polycrystalline nature of microbars. The exchange stiffness parameter A was set to $9 \times 10^{-12} \text{ J m}^{-1}$, while the damping coefficient α was set to 0.1. Simulations were stopped when the residual torque fulfilled the condition: $|\vec{m} \times \vec{H}| < 10^{-6}$. Two shapes were used for modeling, a microbar with ideally smooth edges and oval corners, and the actual AFM image of an AR 5.00 microbar with some edge roughness and oval corners with slight irregularities. Each cell used for calculation encompassed a template area of 5×5 pixels. The results of micromagnetic modeling are presented in Fig. 5a, together with the remanent magnetization curve for AR 5.00 microbars, from Fig. 3f. Several characteristic micromagnetic configurations are presented in Figs. 5b–e.

The remanent magnetization curve shows that the standard deviation the switching field of AR 5.00 microbars is 50 Oe from the nominal coercivity of 115 Oe. Successful modeling therefore should recover the coercivity within one standard deviation from the nominal value. Fig. 5(a) demonstrates very good agreement between the remanent magnetization curve (solid line) and the simulated magnetization curve for a microbar with rough edges (dashed line), but not particularly good agreement with the simulated magnetization curve for a microbar with smooth edges (dotted line).

The simulation predicts that the magnetization reversal of a microbar with smooth edges proceeds through formation of two vortices of opposite chirality at the oblique ends. As the area affected by vortex magnetization expands towards the center of the microbar, the edges of the vortices meet to form a central, transverse head to head domain wall [18]. The magnetization then rotates in the direction of the applied field. As the coercivity of the resulting magnetization curve (~ 30 Oe) deviates more than one standard deviation from the coercivity of the remanent magnetization curve, the switching of the AR 5.00 microbar most likely does not proceed via formation of a head-to-head wall.

Much better agreement with the remanent magnetization curve was obtained when the ideal bar used for micromagnetic simulation was replaced with an actual AFM image of AR 5.00 microbar, dashed line in Fig. 5(a). The higher observed coercivity of the microbar was probably a result of magnetization pinning at the rough edges by the edge domains [19]. According to the micromagnetic simulation, the reversal starts when a vortex core appears at the edge of one of the oblique ends of the microbar. The vortex core then creates an area of reversed magnetization, anti-parallel to the magnetization along the edges. At that point, magnetization along the edges is still parallel to the initial magnetization direction. The region of the reversed magnetization expands towards the other side of the bar through formation of vortex cores of alternating chirality at the edge. The vortex cores of alternating chirality propagate perpendicularly to the direction of the applied field toward the opposite

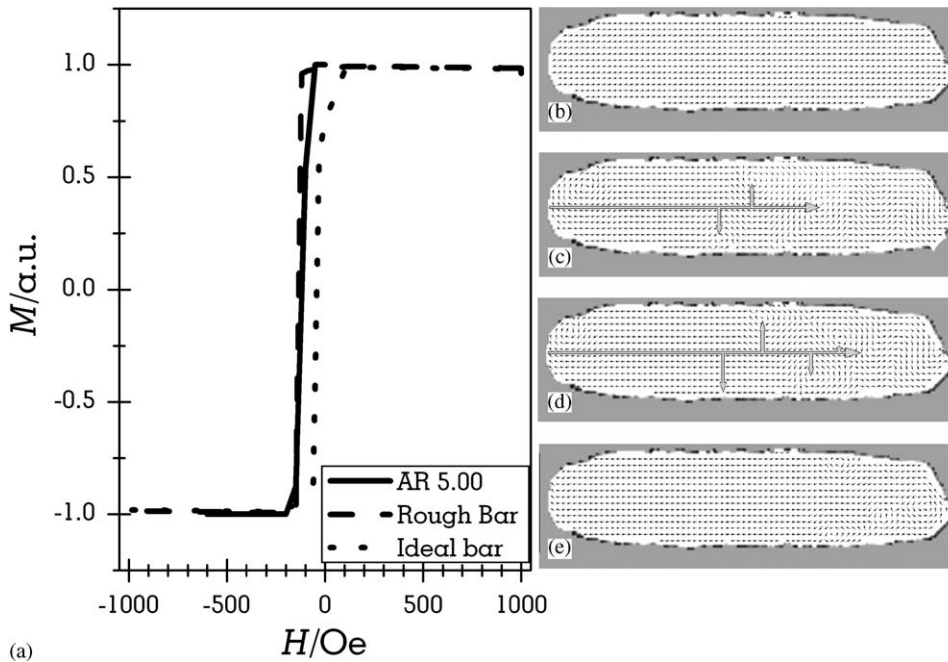


Fig. 5. (a–e) Comparison of experimental (solid line) with the simulated magnetization curves for two microbars with characteristic edges: a microbar with smooth (dotted line) and rough edges (dashed line), Fig. 5a. Fig. 5b–e represents magnetization configurations resulting from the simulation of a microbar with rough edges at: (b) +1 kOe, (c) and (d) –120 to –150 Oe, i.e., transitional magnetization states, and (e) –1 kOe. Long arrows in (c) and (d) point towards the edge of the reversed magnetization region in the direction of reversal propagation, while smaller lateral arrows point to the centers of vortex cores originating along the transverse line in the direction of vortex core propagation.

edges of a microbar, leaving behind the areas with reversed magnetization (see schematics in Figs. 5(c) and (d)). The coercivity of the simulated magnetization curve for a microbar with rough edges was 135 Oe, which was within one standard deviation of the coercivity of the remanent magnetization curve (115 Oe). Furthermore, the magnetization reversal mechanism can be extrapolated to the microbars with smaller aspect ratios, because their coercivities were lower than the ones predicted by the coherent rotation theory.

The remanent magnetization curves calculated from the MFM study were also compared to the remanent magnetization curve measured for the entire sample by the VSM bulk magnetization measurement. In order to calculate total remanent magnetization of the sample from the corresponding MFM images, the total number of bars with negative magnetization was subtracted from the total number of bars with positive magnetization,

and the result divided by the total number of bars in the image. Calculated (solid circles) and measured (solid line) remanent magnetization curves are presented in Fig. 6, together with the magnetization curve of the entire sample (sweeping field range ± 1 kOe, parallel to the sample surface).

There is very good agreement between the MFM and VSM remanent magnetization curves between 0 and –350 Oe. At fields more negative than –350 Oe there is about 10% discrepancy between the MFM and VSM curves, but both curves follow the same trend. The discrepancy between the remanent magnetization curves and the magnetization curve indicates that some of the microbars that were in a single-domain state in the applied field resumed a domain closure state at the remanence.

Good agreement between the measured and calculated remanent curves validates the utilization of MFM images for calculation of remanent

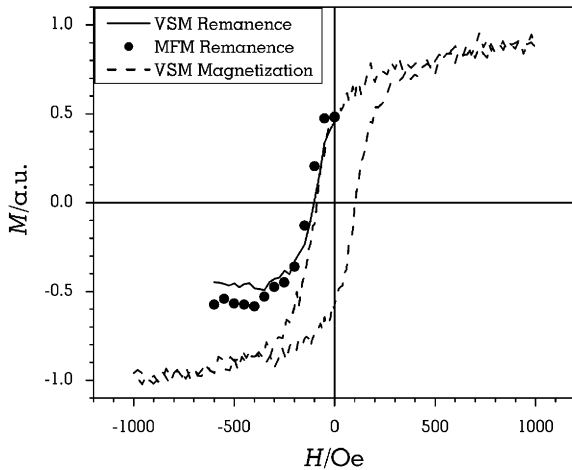


Fig. 6. The net MFM remanent magnetization curve (solid circles) compared to the VSM remanent magnetization curve (solid line) and the VSM magnetization curve (dashed line). The VSM magnetization curve was obtained by measuring magnetization while sweeping the field parallel to the sample surface in the (+1000, –1000) Oe range. The MFM curve was normalized with respect to the total number of nickel microbars in one image, while VSM curves were normalized with respect to the saturation magnetization determined from the VSM magnetization curve.

magnetization curves for microbars with various aspect ratios, as given in Figs. 3a–f.

3.5. Stability of vortex states

The magnetization states of microbars with a given aspect ratio at the remanence are an important indication of the prevailing magnetization state, single domain versus flux closure (demagnetized). As a measure of the tendency of microbars to retain the single-domain state, the fraction of microbars in a single-domain state after field reversal to -100 Oe was measured at the remanence. The number of microbars in a single-domain state, regardless of their orientation, was divided by the total number of microbars to calculate the percentage of demagnetized microbars. The results for all six aspect ratios are presented in Fig. 7.

According to Fig. 7 almost 90% of AR 1.43 microbars are in a demagnetized state at the remanence. Zero magnetization is achieved through the magnetic flux closure within the

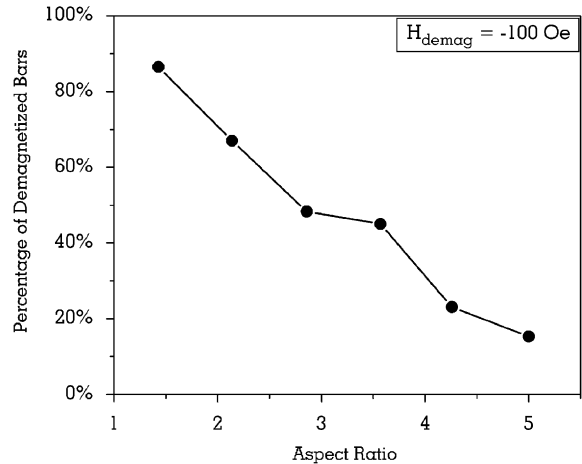


Fig. 7. Effect of aspect ratio on the percentage of demagnetized microbars at the remanence, after applied reverse field of -100 Oe. Percentage calculated from microbars counted in the corresponding MFM image.

microbar. As the aspect ratio increased, the fraction of microbars in the demagnetized state decreased. For example, about 15% of AR 5.00 microbars were found in a demagnetized state. By comparing these results with those from the study of cobalt microbars [11], it should be noted that: (a) the coercivity of cobalt microbars was higher (~ 200 Oe); and (b) AR 5.00 cobalt microbars could not be found in a demagnetized state. The existence of nickel AR 5.00 microbars in a demagnetized state is probably a consequence of their lower magnetostatic energy, due to the lower magnetic moment of nickel.

4. Conclusions

1. In an externally applied field, nickel microbars assumed a single-domain magnetization state.
2. A correlation between the width of the switching field range to the shape anisotropy, defined according to length-to-width aspect ratio, was established.
3. Micromagnetic modeling revealed that magnetization reversal takes place through vortex generation from a central region of reversed magnetization. The coercivity was lower than

the one predicted by the coherent spin rotation mechanism, but higher than the one for the transverse wall formation mechanism. Magnetization along the edges was pinned by the edge domains.

4. There is a good agreement between the remanent magnetization curves obtained by micro-magnetic analysis (MFM) and macromagnetic characterization (VSM).

Acknowledgements

This work was sponsored by the US Department of Defense, Department of the Navy, Office of Naval Research, Grant Number N000140110829, and The National Science Foundation RII Award (EPS 0132626). Help by Obducat (Malmo, Sweden) during acquisition of nanoimprint equipment and technical training is greatly appreciated.

References

- [1] K. Bussmann, G.A. Prinz, S.F. Cheng, D. Wang, *Appl. Phys. Lett.* 75 (16) (1999) 2476.0.
- [2] J. Raabe, R. Pulwey, R. Sattler, T. Schweinbock, J. Zweck, D. Weiss, *J. Appl. Phys.* 88 (7) (2000) 4437.
- [3] X. Zhu, P. Grutter, V. Metlushko, B. Ilic, *App. Phys. Lett.* 80 (25) (2002) 4789.
- [4] J.A. Johnson, M. Grimsditch, V. Metlushko, P. Vavassori, B. Ilic, P. Neuzil, R. Kumar, *Appl. Phys. Lett.* 77 (26) (2000) 4410.
- [5] W. Xu, J. Wong, C.C. Cheng, R. Johanson, A. Scherer, *J. Vac. Sci. Technol. B* 13 (6) (1995) 2372.
- [6] S.P. Li, A. Lebib, Y. Chen, Y. Fu, M.E. Welland, *J. Appl. Phys.* 91 (12) (2002) 9964.
- [7] C.A. Ross, M. Hwang, M. Shima, J.Y. Cheng, M. Farhoud, T.A. Savas, H.I. Smith, W. Schwarzacher, F.M. Ross, M. Redjail, F.B. Humphrey, *Phys. Rev. B* 65 (2002) 144417.
- [8] A. Robinson, W. Schwarzacher, *J. Appl. Phys.* 93 (10) (2003) 7250.
- [9] M. Vazquez, K. Pirota, M. Hernandez-Velez, V.M. Prida, D. Navas, R. Sanz, F. Batallan, J. Velazquez, *J. Appl. Phys.* 95 (11) (2004) 6642.
- [10] M.S. Wei, S.Y. Chou, *J. Appl. Phys.* 76 (10) (1994) 6679.
- [11] D. Grujicic, B. Pesic, *J. Magn. Mater.* in press.
- [12] G. Bochi, C.A. Bellentine, H.E. Inglefield, C.V. Thompson, R.C. O'Handley, *Phys. Rev. B* 53 (4) (1996) R1729.
- [13] R. Vollmer, Th. Gutjahr-Loser, J. Kirschner, S. van Dijken, B. Poelsema, *Phys. Rev. B* 60 (9) (1999) 6277.
- [14] B.D. Cullity, *Introduction to Magnetic Materials*, Pearson Addison-Wesley, Boston, MA, 1972, p. 614.
- [15] J. Shi, J. Li, S. Tehrani, *J. Appl. Phys.* 91 (10) (2002) 7458.
- [16] E.C. Stoner, E.P. Wohlfarth, *Philos. Trans. Roy. Soc. A* 240 (1948) 599.
- [17] M.J. Donahue, D.G. Porter, *OOMMF User's Guide*, Version 1.0, Interagency Report NISTIR 6376, NIST, Gaithersburg, MD (September 1999). url: <http://math.nist.gov/oommf>.
- [18] R.D. McMichael, M.J. Donahue, *IEEE Trans. Magn.* 33 (1997) 4167.
- [19] R.D. McMichael, J. Eicke, M.J. Donahue, D.G. Porter, *J. Appl. Phys.* 87 (9) (2000) 7058.